A reconstruction of charge movement during the action potential in frog skeletal muscle

Christopher L.-H. Huang,* and Lee D. Peachey‡

*Physiological Laboratory, Downing Street, Cambridge, United Kingdom; and ‡Leidy Laboratory of Biology, College of Arts and Sciences, University of Pennsylvania, Philadelphia, Pennsylvania 19104, USA

ABSTRACT The transfer of intramembrane charge during an action potential at 4°C was reconstructed for a model representing the electrical properties of frog skeletal muscle by a cylindrical surface membrane and 16 concentric annuli ("shells") of transverse tubular membrane of equal radial thickness. The lumina of the transverse tubules were separated from extracellular fluid by a fixed series resistance. The quantity, geometrical distribution and steady-state and kinetic properties of charge movement components were described by equations incorporating earlier experimental results. Introducing such nonlinear charge into the distributed model for muscle membrane diminished the maximum amplitude of the action potential within the transverse tubules by 2 mV but increased the maximum size of the after-depolarization by 3–5 mV and also its duration. However, these changes were small in comparison to the 135-mV deflection represented by the action potential. They therefore did not justify altering the values of the electrical parameters adopted by Adrian R.H., and L. D. Peachey (1973. *J. Physiol. [Lond.].* 235:103–131.) and used in the present calculations.

Cable properties significantly affected the time course and extent of charge movement in each shell during action potential propagation into the tubular system. Q_β charge moved relatively rapidly in all annuli, and did so without significant latency ($\approx$0.3 ms) after the surface action potential upstroke. Its peak displacement varied between 53 and 58% (the range representing the difference fiber edge/fiber axis) of the total Q_β charge. This was attained at 5.4–7.3 ms after the stimulus, depending on depth within the tubules. In contrast, q_γ moved after a 1.7–2.9 ms latency and achieved a peak displacement of up to 22–34% of available charge. Both charge movement species could be driven by repetitive (47.7 Hz) action potentials without buildup of charge transfer. Such stimulus frequencies would normally cause tetanus.

Latencies in q_γ charge movement in response to an action potential were resolved into (*a*) propagation of tubular depolarization required to gain the "threshold" of q_γ charge (0.8–1.5 ms) and (*b*) dielectric loss processes. The latter took consistently around 1.5 ms throughout the tubular system. Taken with (c) the earlier reports of a minimal latency in $\Delta[Ca^{2+}]$ signals attributed to tubulo-cisternal coupling following voltage sensing (~2 ms: Zhu, P.H., I. Parker, and R. Miledi., 1986. *Proc. R. Soc. Lond. B. Biol. Sci.* 229:39–46.) these times can be reconciled to the latency (~4–5 ms) reported between the onset of the surface action potential and that of $\Delta[Ca^{2+}]$ signals (Vergara, J., and M. Delay. 1986. *Proc. R. Soc. Lond. B. Biol. Sci.* 229:97–110.). This is consistent with a relationship between the q_γ system and excitation-contraction coupling whether as an independent event (e.g., Adrian, R.H., and C.L.-H. Huang. 1984. *J. Physiol. (Lond.).* 353:419–434.) or as an end reaction following earlier (q_β) transfers of charge (e.g., Horowicz, P., and M.F. Schneider. 1981. *J. Physiol. (Lond.).* 314:565–593.; Melzer, W., M.F. Schneider, B.J. Simon, and G. Szucs. 1986. *J. Physiol. (Lond.).* 373:481–512.)

INTRODUCTION

Adrian and Peachey (1973) reconstructed the form and propagation of an action potential along the surface and tubular membranes of frog skeletal muscle. They employed available experimental descriptions of the kinetic and steady-state properties of Na, K, and leak ionic currents (Adrian et al., 1970), and of the transverse tubular system (e.g., Peachey, 1965; Adrian et al., 1969*a*, 1969*b*). Particular values were assumed for the access resistance, R_s, that separated the extracellular fluid from the transverse tubule lumina, and of the relative densities of ionic channels in surface and tubular membranes. This approach not only reproduced the form of the surface action potential, including its prolonged after-depolarization and its conduction velocity along the fiber surface (cf Gage and Eisenberg, 1969*a*, *b*), but also provided a description of the electrical waveforms that took place within the transverse tubules at various depths within the fiber.

These calculations and the existing available equivalent circuits (see e.g., Eisenberg, 1983) for muscle membranes assumed that the surface and transverse tubular capacitances were independent of membrane potential and showed ideal (nonlossy) charging behavior. More recently, intramembrane charge movements have been demonstrated in skeletal muscle by employing

Address correspondence to Dr. Huang.

0006-3495/92/05/1133/14 $2.00

voltage clamp steps to varying test voltages under conditions when ionic membrane currents were minimized (Schneider and Chandler, 1973; Chandler et al., 1976*a, b*). Such charge could as much as double the membrane capacitance at certain voltages, as compared to the values observed near the resting potential (Adrian and Almers, 1976*a, b*) in addition to introducing additional dielectric loss characteristics into the muscle membrane (Huang, 1981*a,* 1983*b*). Indeed, an examination of a wide range of membrane potentials revealed that up to 70% of the measured capacitance arose from nonlinear rather than linear charge at some voltages (Huang, 1981*b;* Duane and Huang, 1982).

These more recent findings pose fresh questions amenable to further modeling studies. Such additional capacitative loads could alter action potential form and propagation. The existing experimental information on charge movements bears only upon their responses to voltage clamp steps and not to surface or tubular action potentials which would constitute their actual stimulus in vivo. Recent evidence suggests an involvement of some or all of the charge movement in triggering excitation-contraction coupling in skeletal muscle (Huang 1981*c,* 1982; Hui, 1983; Horowicz and Schneider, 1981; Brum and Rios, 1987). Useful insights would therefore emerge from relating the waveforms of action potentials and of the resulting charge movements to those of intracellular $\Delta[Ca^{2+}]$ signals reflecting consequent Ca^{2+} release.

This paper extends the approach described by Adrian and Peachey (1973) to predict intramembrane charge transfers during an action potential initiated in the surface membrane and the outer regions of the transverse tubules and then allowed to propagate into the tubular system. This study was, in part, prompted by earlier studies (Huang and Peachey, 1988, 1989) that characterized the relative distribution of components of the nonlinear charge over the tubular and surface membranes in which it was shown experimentally that the charge q_β is evenly distributed over surface and transverse tubular membranes and that q_γ is distributed in the tubular system only. This enables estimates to be made of the contributions of intramembrane charge to the surface and each element of the tubular cable system in a model such as that used by Adrian and Peachey (1973). We first examined whether introducing nonlinear membrane capacitance significantly alters the form of the action potential as predicted by Adrian and Peachey (1973). This was done particularly as the earlier work had assumed values for the series resistances and for relative ionic channel distributions between surface and tubular membranes that were feasible for surface and tubular system membranes without nonlinear capacitances. The expected behavior of the different charge components through different regions of the transverse tubules during a single action potential was then computed. Finally, the effect of repetitive firing at frequencies that would have been sufficient to produce tetanus in vivo was examined. This was done to see if the predicted charge movements could be considered as sufficient and appropriate for contraction activation according to present models of excitation-contraction coupling. Preliminary abstracts of some of the findings have been presented (Huang and Peachey, 1989; 1990).

THEORY

Fiber and tubular geometry

Formalisms already described in earlier work (Adrian and Peachey, 1973) are outlined only, principally to define and state particular numerical values chosen here. Kinetic equations, where introduced, will designate forward and backward rate constants by the symbols A and B, respectively, as the usual symbols α and β have also been used to denote charge movement components by Adrian and Peres (1979). We solved for the membrane potential and for the ionic and capacity currents that would flow through the course of an action potential initiated in the surface membrane and the outer rim of the transverse tubules, and allowed to propagate into the remaining tubular system.

If one assumes internal isopotentiality and linear membrane properties, then the potential, V, across any element at time, t, and distance r from the fiber axis relative to the external potential is given by the differential equation (Adrian et al., 1969*a, b*):

$$\frac{1}{r}\cdot\frac{\partial}{\partial r}\frac{(r\partial V)}{\partial r}=\frac{\overline{G}_W V}{\overline{G}_L}+\frac{\overline{C}_w}{\overline{G}_L}\cdot\frac{\partial V}{\partial t}. \quad (1)$$

The volume-specific parameters $\overline{G}_L$, $\overline{G}_W$, and $\overline{C}_W$ are determined by values of the tubule lumen conductivity G_L, and the conductance G_W and the capacitance C_W respectively of 1 cm^2 of tubular membrane, and by the following tubular geometric parameters: ρ, the fraction of muscle volume occupied by tubules, ζ, the volume/surface ratio of the tubules, and σ, the network geometric factor:

$$\overline{G}_L = G_L\rho\sigma \quad (2)$$

$$\overline{G}_W = G_W\rho/\zeta \quad (3)$$

$$\overline{C}_W = C_W\rho/\zeta. \quad (4)$$

The present study assumed a fiber radius of $a = 55$ μm, for which it is known that $\rho = 0.003$, and the values $\zeta = 10^{-6}$ cm (Peachey, 1965), $\sigma = 0.5$, $C_W = 1$ $\mu F/cm^2$, $G_L =$

10 mmho/cm (Adrian et al., 1969*a*), and G_W = 0.0067 mmho/cm^2 (Adrian and Peachey, 1973: their Table 1 *B*).

Access resistance to the transverse tubules

An access resistance R_s may separate the transverse tubular lumina from the extracellular fluid. This sets a boundary condition for Eq. 1 above at $r = a$ that involves the radial tubular luminal current across this access resistance. If V_a is the membrane potential across the wall of the transverse tubular system at the inner end of the access resistance:

$$(V - V_a) = R_s \bar{G}_L \left.\frac{\partial V}{\partial r}\right|_{r=a}. \quad (5)$$

We assumed a value for the access resistance, R_s = 100 Ω.cm^2 (Adrian and Peachey, 1973).

Nonlinear ionic currents

Next, nonlinear membrane currents were incorporated into the circuit elements organized into surface and tubular membrane systems. The analysis here considered both ionic and capacitative currents. Over the timecourse of an action potential, the ionic current I_i across any membrane element, j, is the sum of Na, K, and leak currents. Dropping the subscript j for simplicity, this would be given by:

$$I_i = g_T(V - V'_L) + g_{Na}(V - V'_{Na}) + g_K(V - V'_K), \quad (6)$$

where the g's represent leak, Na, K membrane conductances respectively. The equilibrium potentials were set at:

$$V'_L = -95 \text{ mV}, V'_{Na} = 50 \text{ mV and } V'_K = -85 \text{ mV}.$$

The sodium and potassium conductances were given by the equations:

$$g_{Na} = \bar{g}_{Na} m^3 h \quad (7)$$

$$g_K = \bar{g}_K n^4 \quad (8)$$

The maximum conductances $\bar{g}_{Na}$, $\bar{g}_K$, and the Hodgkin-Huxley variables m, n, and h were defined for surface and tubular membrane assuming a temperature of 4°C and a temperature coefficient of 2.5. Equations for their first-order rate constants were obtained from Table 6 *A* of Adrian et al. (1970). Values for the constants in these equations were obtained from Table 6 *B* of Adrian et al. (1970) and Table 1 *A*, column 4 of Adrian and Peachey (1973).

Nonlinear capacitative charge

The present calculations incorporate the capacitative contributions made by charge movements (Schneider and Chandler, 1973; Adrian and Almers, 1976*a, b;* Chandler et al., 1976*a, b*). These alter the steady-state charge stored by the membrane and can contribute dielectric loss transients (Huang, 1980, 1981*a,* 1983*a, b*). Effects primarily arising respectively from steady-state or from dielectric loss behavior could be distinguished by comparing the predictions from two types of model. The simpler model assumed nonlossy and nonlinear capacitance across which the charge stored would vary instantaneously with imposed voltage. A more realistic model then additionally incorporated dielectric loss behavior described phenomenologically in terms of q_β and q_γ components as determined on earlier occasions using imposed voltage steps (see Adrian, 1978; Almers, 1978; and Huang, 1988, for reviews). The physical interpretation of such a descriptive treatment, whether in terms of a single sequence of events (Brum and Rios, 1987) or as parallel independent processes (Adrian and Huang, 1984*b*), is considered elsewhere (Huang, 1986, 1987; Hui and Chandler, 1991).

In the steady state, at any given membrane voltage V, the amount of q_β charge is:

$$Q_\beta = \hat{Q}_\beta / [1 + \exp[-(V - \bar{V}_\beta)/k_\beta]], \quad (9)$$

The term $\hat{Q}_\beta$ is the maximal transferable quantity of q_β in $nC/\mu F$ in that element of membrane at membrane potential V. We adopted values of the transition voltage $\bar{V}_\beta = -26$ mV and steepness factor k_β = 15 mV (Almers, 1976). A number of formalisms (Adrian and Peres, 1977; Hui, 1983; Huang, 1984) are also available to describe the q_γ charge. We have chosen the fourth-order form introduced by Adrian and Peres (1977):

$$Q_\gamma = \hat{Q}_\gamma n_\infty^4. \quad (10)$$

This provides a relatively simple descriptive equation suitable for preliminary modelling. Additionally, n_∞ is also the steady-state solution as a function of voltage for the Hodgkin-Huxley variable n for the K^+ conductance. The latter is described by first order rate equations whose respective forward and backward rate constants (in ms^{-1}) are given in Tables 6 *A* and 6 *B* of Adrian et al. (1970):

$$A_n = 0.0044 (V + 46)/[1 - \exp[-(V + 46)/7]] \quad (11)$$

$$B_n = 0.01848 \exp[-(V + 46)/40]. \quad (12)$$

In the steady state, or where one assumes nonlossy capacitative contributions from the q_β and q_γ charges, the capacitance C_{eff} of any given membrane element, j, is

related to its control value C_m by,

$$C_{eff} = C_m(1 + C'_\beta + C'_\gamma), \quad (13)$$

again dropping the subscript j for simplicity. The q_β and q_γ terms are then obtained by differentiating Eqs. 9 and 10 above:

$$C'_\beta = \hat{Q}_\beta/[2k_\beta[1 + \cosh(-(V - \overline{V}_\beta)/k_\beta)]]. \quad (14)$$

$$C'_\gamma = \hat{Q}_\gamma \cdot [d(n_\infty^4)/dV]. \quad (15)$$

The model incorporating dielectric loss expressed capacitative currents due to q_β and q_γ as the differential equations (see Adrian, 1978):

$$dQ_\beta/dt = A_\beta(\hat{Q}_\beta - Q_\beta) - B_\beta Q_\beta. \quad (16)$$

The respective forward and backward rate constants are most concisely expressed as:

$$A_\beta = \overline{A}_\beta \Phi_\beta/[1 - \exp(-\Phi_\beta)], \quad (17)$$

and

$$B_\beta = A_\beta/\exp(\Phi_\beta), \quad (18)$$

where $\Phi_\beta = -(V - \overline{V}_\beta)/k_\beta$, and the constant $\overline{A}_\beta$ = 0.051/ms, as obtained from Adrian (1978). For the q_γ component,

$$dQ_\gamma/dt = 4\hat{Q}_\gamma n^3[A_n(1 - n) - B_n n]. \quad (19)$$

This assumes the standard form for the differential of a function of a function. A_n and B_n are the rate constants for the Hodgkin-Huxley variable n defined by Eqs. 11 and 12.

Distribution of linear elements in tubular membrane

Following Adrian and Peachey (1973), we calculated action potentials and related changes while avoiding integration over the radial distance r by dividing the tubular system into $N = 16$ sections of equal radial thickness consisting of a central disk ($j = 1$) and 15 concentric annuli or 'shells' ($j = 2$ to 16). For a fiber of radius a, the volume of each shell in unit muscle fiber length is then $\pi a^2(2j - 1)/N^2$, and this accounts for a fraction,

$$\bar{v}_j = (2j - 1)/\sum_{j=1}^{N}(2j - 1), \quad (20)$$

of both muscle volume and total available tubular surface area. The linear tubular conductances $g_{T(j)}$ and capacitances $C_{T(j)}$ of each shell, j, were then calculated assuming constant specific conductances and capacitances using Eqs. 2–4 and were normalized to unit fiber length. In the present calculations, the latter represents the most economical dimensional form. Radial conductances $g_{L(j)}$ between the centers of adjacent annuli were similarly calculated, with $g_{L(16)}$ including the access resistance between the outermost tubular annulus and the extracellular fluid. It was assumed that ionic conductances in surface and transverse tubular membrane had similar kinetic properties but different respective limiting values $\bar{g}_{Na}$, $\bar{g}_K$, as described by Adrian and Peachey (1973: Table 1 *A*, column 4, and Table 1 *B*, column 2), and Adrian et al. (1970: Table 6 *A*, and Table 6 *B*, column 3).

Distribution of nonlinear charge in tubular and surface membranes

Experimental values of $Q_{\beta max}$ and $Q_{\gamma max}$, the maximum available q_β and q_γ charge, are available in units of $nC/\mu F$ of linear membrane capacitance (Adrian and Peres, 1979; Huang, 1982; Hui, 1983). However, the present computations required these electrical quantities to be normalized to unit fiber length. This change in units required a computation which involved the linear capacitance of unit fiber length of tubular system as well as the surface capacitance. On the lattice scheme for tubular geometry adopted here (Adrian et al., 1969*a*) the tubular term in the total capacitance of unit membrane surface area, C_{tot}, requires a value of tubular capacitance of unit volume. This latter term is a function of the fiber radius a. Thus if one assumes a uniform specific capacitance C_W through surface and tubular membrane systems:

$$C_{tot} = C_W + [(a\rho C_W/(2\zeta)]. \quad (20a)$$

This gives rise to the following ratios between capacitative contributions between different regions of membrane:

(tubular capacitance)/(total capacitance)

$$= [1 + 2\zeta/(a\rho)]^{-1} \quad (20b)$$

(surface capacitance)/(total capacitance)

$$= [1 + a\rho/(2\zeta)]^{-1} \quad (20c)$$

The sets of equations (20*a–c*) are important when considering the relative densities of each charge species in surface and tubular membranes. Huang and Peachey (1988, 1989) suggested that the q_γ component occurs primarily in the tubular membrane, in contrast to an even distribution of q_β over the surface and tubular membrane capacitances. In addition, the amount of q_γ charge referred to unit fiber surface area is linearly related to fiber diameter (Adrian and Huang, 1984*b*).

This suggests in addition a uniform density of q_γ through the tubular membrane. The maximum q_γ charge $\hat{Q}_{\gamma(j)}$ in any shell j would then be proportional to the volume of the shell expressed as a fraction $\bar{v}_j$ of the total fiber volume, and to $Q_{\gamma max}$ in $nC/\mu F$ of linear membrane (both tubular and surface) capacitance obtained from a fiber of the same diameter. If $\hat{Q}_{\gamma(j)}$ refers to unit fiber length, it must then refer to a linear membrane capacitance of $2\pi a C_{tot}$ (see Eq. 20*a*). Thus, assuming that q_γ occurs exclusively in the tubules:

$$\hat{Q}_{\gamma(j)} = Q_{\gamma max} C_{tot} 2\pi a \bar{v}_j; \quad 1 \le j \le N$$
$$= 0 \quad j = N + 1. \tag{21}$$

Expressions for the maximum charge $\hat{Q}_{\beta(j)}$ in unit fiber length for surface ($j = N + 1$) and tubular ($1 \le j \le N$) shells assumed an even distribution of q_β referred to unit linear surface and tubular membrane capacitance. The q_β charge is thus allocated between tubular and surface membranes using the ratios in Eqs. (20*b–c*). The amounts of q_β charge in each shell j can be calculated, thus:

$$\hat{Q}_{\beta(j)} = Q_{\beta max} C_{tot} (2\pi a) \bar{v}_j [1 + 2\zeta/(a\rho)]^{-1}; \quad 1 \le j \le N$$
$$= Q_{\beta max} C_{tot} (2\pi a) [1 + a\rho/(2\zeta)]^{-1}; \quad j = N + 1. \tag{22}$$

Several papers provide estimates for $Q_{\beta max}$ and $Q_{\gamma max}$ (Adrian and Peres, 1979; Huang, 1982; Hui, 1983). We adopted the values $Q_{\beta max} = 20\ nC/\mu F$ and $Q_{\gamma max} = 15\ nC/\mu F$ (Huang, 1982) as fiber radii in that study were similar to that modeled here.

Cable formulation for nonlinear tubular system

The relationships between membrane potential and currents flowing through or across the tubular system for different types of model now emerge immediately. The control model assuming a linear membrane capacitance gives the potential V_j across the tubular wall for the first annulus ($j = 1$) by:

$$\frac{dV_1}{dt} = \frac{(V_2 - V_1) g_{L(1)} - I_1}{C_{T(1)}}. \tag{23}$$

For the j^{th} annulus, with $1 < j < (N + 1)$,

$$\frac{dV_j}{dt} = \frac{(V_{j+1} - V_j) g_{L(j)} - I_j - (V_j - V_{j-1}) g_{L(j-1)}}{C_{T(j)}}. \tag{24}$$

The ionic membrane current in each annulus is:

$$I_j = g_{T(j)}(V_j - V'_L) + g_{Na(j)}(V_j - V'_{Na}) + g_{K(j)}(V_j - V'_K). \tag{25}$$

The limiting conductances in the $g_{T(j)}$, $g_{Na(j)}$ and $g_{K(j)}$ terms were calculated as described above.

The introduction of nonlinear but nonlossy capacitance entailed an expansion of the $C_{T(j)}$ term in Eqs. 23 and 24 using Eqs. 9–11 but leaving the Eq. 25 for I_j intact. For $j = 1$:

$$\frac{dV_1}{dt} = \frac{(V_2 - V_1) g_{L(1)} - I_1}{C_{T(1)}(1 + C'_{\beta(1)} + C'_{\gamma(1)})}. \tag{26}$$

For $1 < j < (N + 1)$:–

$$\frac{dV_j}{dt} = \frac{(V_{j+1} - V_j) g_{L(j)} - I_j - (V_j - V_{j-1}) g_{L(j-1)}}{C_{T(j)}(1 + C'_{\beta(j)} + C'_{\gamma(j)})}. \tag{27}$$

The charge displaced in any given shell, $Q_{\beta(j)}$, $Q_{\gamma(j)}$ is then given instantaneously by the steady-state Eqs. 14 and 15. In contrast, dielectric loss currents due to q_β and q_γ were most conveniently represented in an explicit way, using a modified form of Eq. 25:

$$I_j = g_{T(j)}(V_j - V'_L) + g_{Na(j)}(V_j - V'_{Na}) + g_{K(j)}$$
$$\cdot (V_j - V'_K) - \frac{dQ_{\beta(j)}}{dt} - \frac{dQ_{\gamma(j)}}{dt} \tag{28}$$

Such a convention enabled Eqs. 23 and 24 to be employed without modification.

METHODS

FORTRAN IV programs were first developed on an IBM-AT micro-computer with a Microsoft-DOS operating system and then transferred to a PDP 11/23 RT-11-V05 SJ system (Digital Equipment Corporation, Maynard, MA) employing an extended instruction set, and with provision for virtual array handling. Unless otherwise stated in the Results, the electrical events were calculated for action potentials induced by a depolarization of duration 0.3 ms imposed to a voltage of −30 mV, delivered to the surface membrane and the membrane of the outermost two annuli (shells) of the transverse tubules, and subsequently propagating into the tubular system. Tubular system was represented by $N = 16$ concentric shells of equal radial widths.

The initial values in the numerical solution employed steady-state parameters for both membrane conductances and capacitances corresponding to a −95 mV resting potential and a temperature of 4°C. Solutions for $Q_{\beta(j)}$, $Q_{\gamma(j)}$, V_j, m_j, n_j, and h_j, described by a matrix of differential equations coupled to a set of subsidiary equations defining the voltage dependence of rate constants for each shell ($j = 1$ to $N + 1$), were obtained (see Theory) employing the Gill modification of a fourth order Runge-Kutta algorithm. The step size was determined at each time increment by a comparison of the set of values of each parameter that was obtained using the stepsize that emerged from the previous iteration, with

the set of values that were obtained using two successive time steps half as large. The stepsize was then appropriately adjusted within the closed interval [0.0004, 1 ms]. Similar numerical procedures have been used by Adrian and Peachey (1973), and Huang (1984).

Results for each shell at 0.3 ms computed time intervals over a 100-ms window after action potential initiation were stored for subsequent display and analysis. Separate programs were developed for models representing systems containing linear, nonlinear and nonlossy, and nonlinear and lossy membrane capacitance respectively (see Theory section).

RESULTS

Reconstruction of surface and tubular action potentials at 4°C

The earlier modeling of action potential propagation along surface membrane and into a distributed tubular system assumed a temperature of 20°C. It employed values for the tubular access resistances and ionic channel distributions that would best fit a system for which membrane capacitances were assumed to be linear (Adrian and Peachey, 1973). However, charge movements have a marked influence upon the effective membrane capacitance at some voltages (Adrian and Almers, 1976a). Accordingly, we considered the extent to which intramembrane charge in a distributed tubular system would affect action potential form. This would determine whether the electrical parameters used in the original modeling by Adrian and Peachey (1973), without nonlinear capacitance, would require reappraisal.

A temperature of 4°C, rather than 20°C, was chosen because charge movements were originally characterized in cooled fibers (see Adrian, 1978; Huang, 1988). At present there is little specific information on their temperature dependence upon which any extrapolation to higher temperatures would depend. In any case, the ionic currents involved were also originally described for cooled fibers: the reconstruction of in vivo events at 20°C assumed a particular temperature dependence (Adrian et al., 1970).

Fig. 1 illustrates the computed action potential at the surface membrane and across tubular membrane at the fiber axis after propagating through the transverse tubules. The surface wave showed an artefact resulting from the stimulus and reached its overshoot beyond +42 mV in less than 1.5 ms after the stimulus. The fast phase in its recovery was then followed by a relatively prolonged after-depolarization extending beyond 100 ms. In contrast, the response at the fiber axis (Fig. 1 *B*) developed more slowly to a later peak near 4 ms, reflecting the time required for the surface wave to propagate to the center of the tubular system. The tubular trace is also broader and its after-depolarization more prolonged. It is pointed out below that this slower tubular waveform is important in determining the extent of charge movement, particularly q_γ. The peak of the tubular action potential fell within 5 mV of its surface value.

Effect of nonlinear charge on the action potential

To assess the extent to which nonlinear charge within the surface and tubular membranes contributes to the form of the action potential, two additional cases were considered. First, voltage-dependent intramembrane

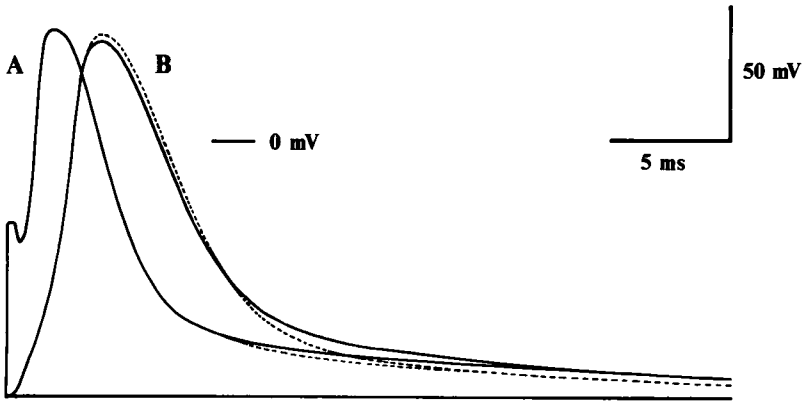

FIGURE 1 Computed surface (*A*) and tubular (*B*) action potentials at the fiber axis in response to a 0.3 ms pulse to −30 mV applied to surface membrane and the outer two annuli (shells) of the transverse tubular system. The trajectories of voltage changes in a model assuming either linear or nonlossy nonlinear membrane capacitances were virtually superimposable. They are indicated by dotted lines where they depart from the timecourse of the voltage change in a lossy nonlinear membrane (*continuous lines*).

charge showing nonlossy behavior was incorporated into the model. Second, rate equations that described the dielectric loss (cf Huang, 1980, 1981*a*, 1983*b*) were introduced into computation (see Theory section). It was therefore possible to identify the consequences of the introduction of nonlinear charge, and then to separate the properties arising from the steady-state and from the dielectric loss characteristics, respectively.

Action potentials calculated for linear and nonlinear nonlossy capacitance were virtually superimposable. They are plotted in Fig. 1 together as dotted lines where their records deviate from the outcome of incorporating dielectric loss (*solid lines*). It is therefore dielectric loss that causes the greater part of any modification of action potential form. At the surface membrane, the overshoot potentials and times to peak were similar in all three cases. Dielectric loss mainly affected later events in the action potential, or electrical changes within the tubules. For example, it slightly diminished the amplitude of the tubular spike and increased the after-depolarization in both tubules and surface membrane. Thus, 30 ms after the initial stimulus, the presence of dielectric loss resulted in a deflection of the after-depolarization by ~2.2 mV relative to the control. Nonlinear capacitance therefore makes a relatively small contribution to the total charging current. Such charge does produce a large change in membrane capacitance (dQ/dV) but this takes place only over a limited voltage range and thus constitutes a small fraction only of the total absolute (linear and nonlinear) capacitative charge. However, the implicit series resistance term introduced by adding lossy properties does slightly damp the voltage oscillation represented by the action potential. Thus it results in a small decrement in surface action potential amplitude and a delay in the tubular voltage decay that follows.

Fig. 2 plots values of the overshoot voltages and times to peak for the action potentials elicited in the surface membrane and in each concentric tubular annulus (shell) for the three cases listed above. The functions that emerged were similar in form. In both cases, there were marked differences in the values observed at the fiber surface and in the outermost regions of the transverse tubules. This finding reflects the partial electrical isolation of the tubular lumen from the extracellular fluid by the series resistance. The surface action potential reached a peak voltage of +41.6 mV at an interval of 1.75 ms after stimulation. Its form was comparable to earlier experimental results obtained at 4°C (Zhu et al., 1986). However, even in the outermost tubular membrane, the peak tubular voltage change was made only to between +30 and +32 mV (depending on the form of the model), and this was attained only after an interval of 2.6 ms after the stimulus. Deeper in the tubular system, the development of the action potential

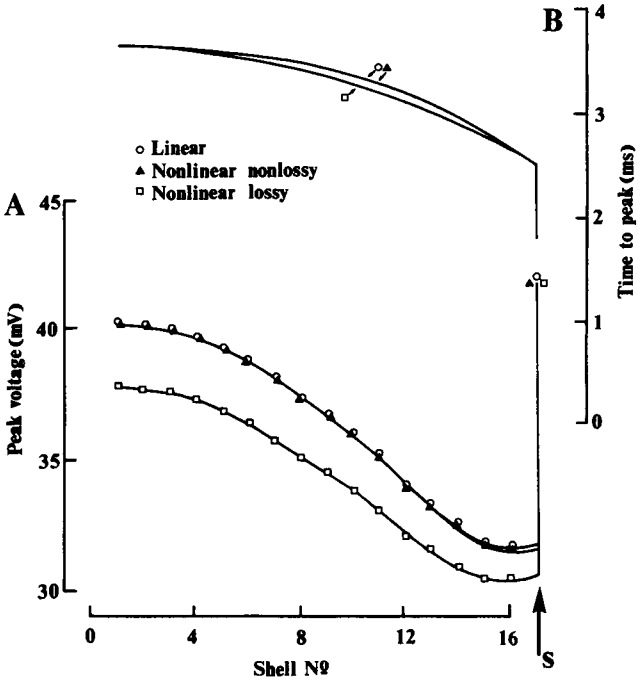

FIGURE 2 Peak voltage deflections (*A*) for action potentials propagated into different transverse tubular annuli (shells) calculated for membrane having a linear capacitance (*circles*), a nonlinear nonlossy capacitance (*triangles*), and a nonlinear lossy capacitance (*squares*). The corresponding symbols also mark times to peak (*B*). Shells of tubular membrane are numbered from 1 (at the fiber axis) to 16 (fiber edge). The last shell is separated from surface membrane (*arrow marked s:* shell 17) by a constant series resistance (cf Adrian and Peachey, 1973).

became more prolonged but the maximum amplitude of the action potential increased. For example, at the fiber axis, the time to peak of the action potential increased to 3.7 ms but its peak voltage increased to between +37.5 and 40 mV. The introduction of nonlinear but nonlossy capacitative charge (Fig. 2, *triangles*) little affected these findings. However, the introduction of dielectric loss (Fig. 2, *squares*) characteristics slightly altered time to peak but more noticeably reduced (by 2–2.5 mV) the maximum overshoot voltage.

Nonlinear capacitance thus caused significant but small changes in the form of computed action potentials, and in their tubular propagation, but not to an extent that would merit altering the parameters originally adopted by Adrian and Peachey (1973), for the present calculations.

Charge transfers within the transverse tubules

The expected displacements of q_β and q_γ charge in each transverse tubular shell were also computed through the

time course of the action potential. Fig. 3 compares the surface action potential (A), with movements of q_β (B) and q_γ (C) charge, normalized to the maximum charge from the respective component available within each shell. Charge movements at the fiber axis are marked S01 to designate the first shell. Similarly, the designations of 4th, 8th, 12th, and 16th shells (denoted by S04, S08, S12, and S16, respectively) refer to annuli counted radially away from the center. The 17th shell designates the surface membrane (S17 in Figs. 3 B and C). The tim course of the charge movement at the surface membrar deviated from the trends shown by charge resident in th tubules. This would reflect the separation of the tubul membrane from the extracellular fluid by the seri resistance, as well as the differing charge distribution For example, both the displacement of q_β charge and i recovery is more rapid at the fiber surface than it is in th tubules. The flat trace shown by the q_γ species in th 17th shell reflects its absence from surface membrar (see Theory section; Huang and Peachey, 1988, 1989).

Fig. 3 demonstrates a greater peak displacement available q_β charge than of q_γ charge by the tubul action potential. Nevertheless, in both cases, there was greater degree of charge transfer at the center than the edge of the tubular system. Figs. 4, C and D, plot th peak charge movement in successive shells of tubul and surface membrane. This function varied smooth with depth within the tubular system. Up to 53% of th available q_β charge moved in the superficial tubules. Th value increased to 58% at the fiber axis (Fig. 4 C). I contrast, tubular propagation had a more marked effe on transfer of q_γ charge. For example, although on 22% of q_γ was displaced in the outer tubules, up to 34

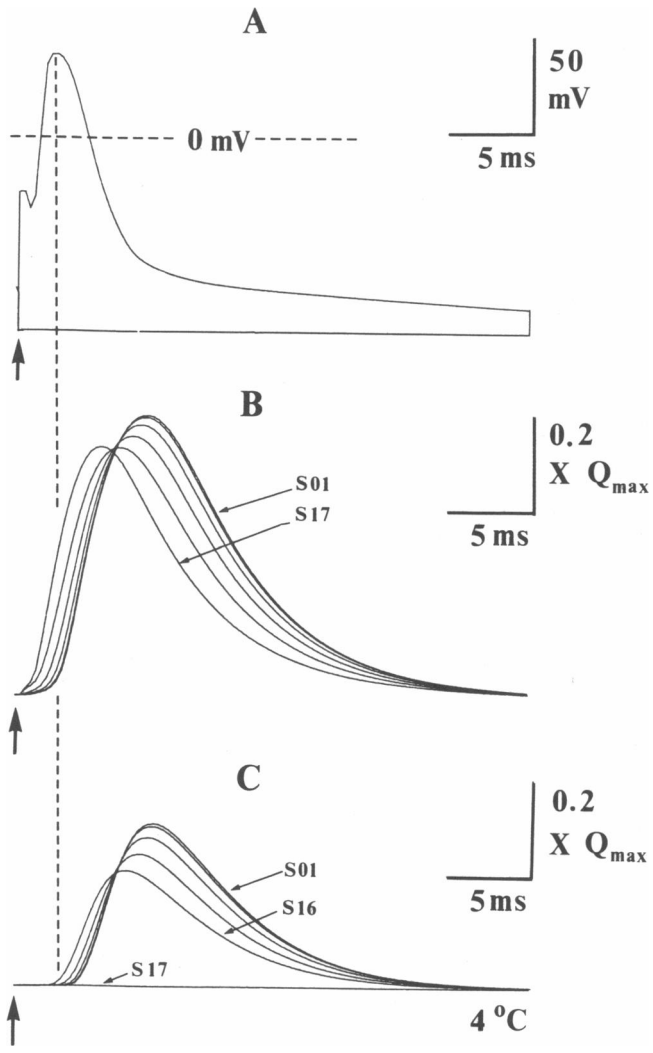

FIGURE 3 The surface action potential (A) compared with the time course of q_β (B) and q_γ (C) charge movement, in individual shells of transverse tubular membrane. Results for the innermost (1st shell, designated S01), 4th, 8th, 12th, 16th, (S04 to S16) tubular shells, and surface membrane (S17) are shown. The arrow denotes time of imposition of the 0.3 ms stimulus to −30 mV. Vertical dotted lines indicate the peak of the surface action potential. Vertical bars in (B) and (C) denote 0.2 times the maximum available charge for each represented shell.

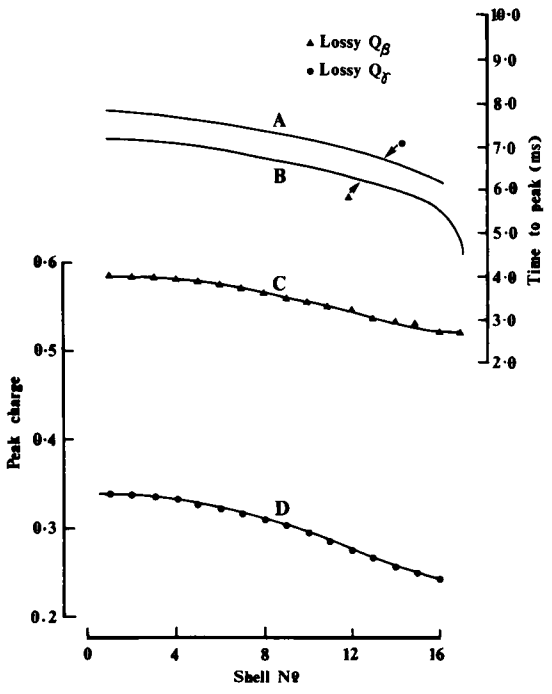

FIGURE 4 Times to peak (A, B) and charge displaced (C, D) as proportion of the maximum available charge in each shell (abscissa) transverse tubular membrane for lossy q_γ (A, D) and q_β (B, C components.

was transferred at the fiber axis (Fig. 4 *D*). The displacements of q_β and q_γ had closer times to peak. These differed between components only by around 0.6 ms consistently throughout the transverse tubular system. Times to peak were longer at the fiber axis (q_γ 7.9 ms, q_β 7.3 ms) than at the perimeter (q_γ 6.14 ms, q_β 5.37 ms). The surface q_β peak was markedly earlier (4.44 ms). The presence of tubular cable properties thus significantly affected both the extent and timecourse of q_β and q_γ charge transfer during action potential generation and propagation in a manner that reflected their different kinetic and steady state properties.

Fig. 1 showed that action potentials are more prolonged within the tubular system at the fiber axis than at the surface. The preceding considerations would account for this greater degree of q_γ transfer in the center of the transverse tubules than at their edge and that this occurs to an extent more noticeable than for the q_β component. Thus, the relatively prolonged time course of tubular action potentials owing to cable propagation preferentially enhances the displacement of q_γ charge.

Latencies of the charge transfers

Fig. 3 shows that noticeable latencies intervene between the onset of the surface action potential and particularly of q_γ charge transfer. It has been suggested that the latter charge triggers Ca^{2+} release from cisternal sarcoplasmic reticulum following membrane depolarization (Huang, 1981*c*; Vergara and Caputo, 1982). Accordingly, it would appear appropriate to compare the latencies in the transfers of nonlinear charge with the latencies for the development of $\Delta[Ca^{2+}]$ signals following the action potential (Vergara and Delay, 1986) as this could offer insights into the possible mechanisms coupling membrane and cisternal events.

Our computations predicted a set of latencies for intramembrane events consistent with the experimental reports, given the hypothesis that the cisternal release of Ca^{2+} in response to an action potential is more directly the consequence of the slower (q_γ) process rather than of q_β charge. The q_β and q_γ latencies for each tubular shell were defined as the time Δt where the trace following charge transfer first departed from the baseline to an extent that exceeded 0.1% of the peak signal, in parallel with the definition adopted by Vergara and Delay (1986) in their description of latencies in Antipyrylazo III absorbance signals used to follow intracellular $[Ca^{2+}]$. Figs. 3, *B* and *C*, illustrate these latencies calculated for different tubular regions. Q_β movements (Fig. 3 *B*) showed little appreciable latency even in regions of the tubular membrane around the fiber axis. In contrast, the greater part of the movement of q_γ charge took place after the peak of the surface action potential (Fig. 3 *C*). Most of the q_γ transition thus relies upon action potentials being more prolonged in the tubular membrane.

The theoretical analysis here throws light on different contributions to the calculated latencies associated with transitions in nonlinear charge. First, there is the time required for action potential propagation into the transverse tubules. Even the transfer of a nonlossy intramembrane charge would require the membrane potential to attain the foot of the appropriate charge-voltage $[Q(V)]$ relation, and a greater depolarization would be required for the q_γ than for the q_β system. Secondly, whereas threshold q_γ transients are prolonged or give rise to humps, q_β currents in response to voltage steps are everywhere simple monotonic decays (Adrian and Peres, 1979; Huang, 1982; Hui, 1983). Fig. 5 separates the overall contributions from such tubular and dielectric loss characteristics for both q_β (Fig. 5 *A*) and q_γ (Fig.

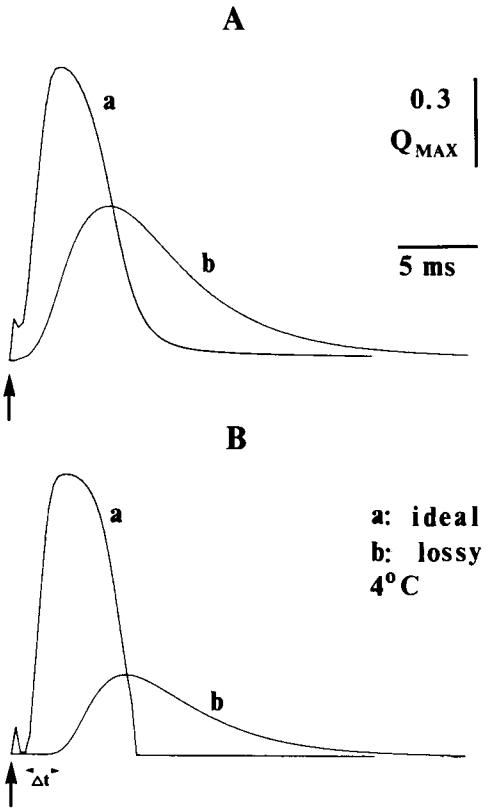

FIGURE 5 Overall movement of q_β (*A*) and q_γ (*B*) charge summated through all tubular shells and surface membrane during an action potential given a model assuming that these components are nonlossy (*a*) or lossy (*b*). The arrow marks the onset of the stimulating pulse. The dielectric loss properties of q_γ result in its showing a larger latency (Δt) than the q_β charge.

5 *B*). The charge movements attributed to each component were summed over all the surface and tubular membrane regions in which they occurred and are displayed normalized to their values of maximum available charge. Findings from both (*a*) nonlossy and (*b*) lossy models for nonlinear charge are shown.

The early artefacts in Figs. 5 *Aa* and 5 *Ba* reflect nonlossy charge transferred instantaneously by the stimulating pulses imposed on surface and outer tubular membranes. On an assumption of nonlossy behavior, an action potential moved virtually all the available nonlinear charge for each component. There was then no significant latency for q_β charge movement, and one close to 0.9 ms for the q_γ species. In contrast, on a hypothesis of lossy capacitative charge, the overall maximum displacement was markedly reduced to 51% (q_β) and 26% (q_γ) respectively. Dielectric loss also prolonged the rising phase of charge transfer. For example, the latency of the lossy q_γ charge movement was prolonged to ~2.2 ms in Fig. 5. The recovery phase was also prolonged beyond the greater part of the time course of the action potential. Finally, dielectric loss characteristics smoothed the overall waveform, particularly of the q_γ charge movement.

Charge movement latencies varied through the tubular system. However, the contribution to these latencies that were the direct consequence of dielectric loss was relatively consistent. Fig. 6 displays these latencies for each concentric shell of tubular membrane, given a lossy (*A*), and a nonlossy q_γ component (*B*), as well as parallel results for the q_β charge (*D* and *E*, respectively). Even a lossy q_β capacitance showed short latencies, and the influence of tubular cable properties made a difference of only 0.32 ms to these times. Such a faster time course would be consistent with the more rapid kinetics of the q_β system. Furthermore, the latter charge has a broader voltage dependence. Consequently, significant q_β charge transfer begins at smaller depolarizations and thus earlier in the time course of the action potential than does q_γ charge movement.

In contrast, even nonlossy q_γ movement had considerably longer latencies: for example, these fell between 1.37 and 0.54 ms for the first and 14th shell respectively (i.e., excluding those shells to which the stimulating voltage step was directly applied). These could be attributed to the times following the stimulus required for tubular transmission and for the voltage to be displaced to the q_γ threshold at any given membrane shell. When assuming lossy intramembrane charge, the q_γ latencies varied between 2.86 ms at tubular membrane situated at the fiber axis to 1.7 ms in membrane at the rim of the tubular system (Fig. 6 *A*). Fig. 6 *C* plots

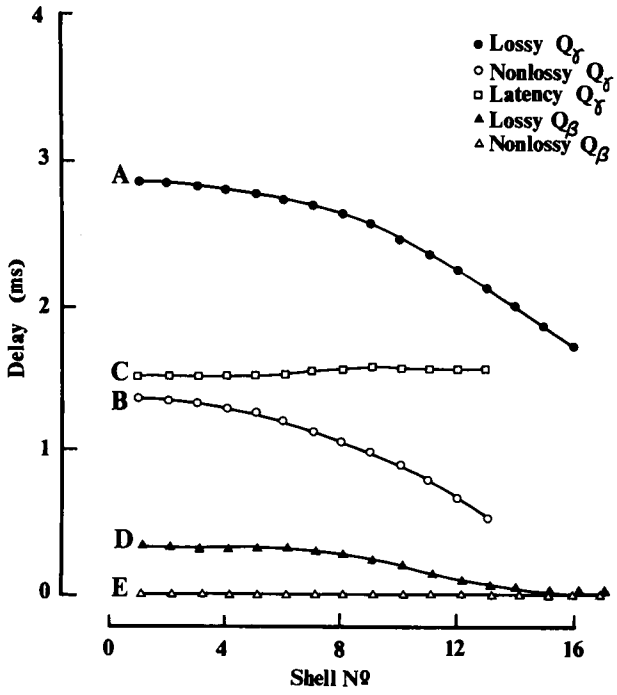

FIGURE 6 Latencies preceding significant movement of q_γ (*A*, *B*) and q_β (*D*, *E*) assuming that these are the consequence of lossy (*A*, *D*) components whose kinetics are defined by equations described in the text, or nonlossy (*B*, *E*) capacitative charge. Delays for a nonlossy model are plotted against shell only for tubular membrane not directly subject to the stimulus used to elicit the action potential (see Methods). The difference (*C*) between lossy and nonlossy predictions given by (*A–B*) indicates the contribution made by dielectric loss in the q_γ delay. The latency has numerically been defined as the time at which the trace following charge transfer first departs from the baseline to an extent that exceeds 0.1% of the peak signal (cf Vergara and Delay, 1986).

the difference (*A–B*) which represents that portion of the latency attributable to dielectric loss. This contribution was ~ 1.5 ms and varied little through the tubular system. This is consistent with earlier reports (Huang, 1981*a*, 1983*b*) of the frequency response characteristics of the q_γ charge. Nevertheless the propagation times through the transverse tubules themselves are responsible for an overall 1.16 ms difference in the latency of the q_γ charge movement between membrane regions at the fiber axis and the fiber rim.

Responses to repetitive stimulation

The repeated suprathreshold stimulation of a muscle fiber above a critical frequency causes progressive fusion of successive twitches resulting in tetanus, to an extent dependent on temperature. The preceding calculations

indicate that a single action potential moves only a fraction of total available charge. However, the modeling studies here made it unlikely that there is any progressive charge buildup during tetanic stimulation. Rather, charge movement appears closely to follow action potentials applied in succession, even at frequencies expected normally to produce tetanus.

The latter result emerged from studies of the extent to which charge movement became cumulative through an action potential train. These modeled the consequences of employing a tetanic stimulation rate of 47.6 Hz in which 1 ms stimulating steps to −30 mV spaced every 20 ms were applied to a five-shell model at a temperature of 4°C. In the course of program execution, the step size in the Runge-Kutta integration was reset to its minimal allowable value with the onset of each stimulating pulse. Values of surface membrane potential V, and of total q_β and q_γ movement were sampled at 0.5 ms intervals. Action potential peaks beyond the first spike were slightly reduced as a result of some Na channel inactivation (Fig. 7 *A*). Higher stimulus frequencies resulted in significant refractoriness. Fig. 7, *B* and *C*, indicate that there was no significant buildup of either q_β or q_γ charge through the stimulus train. Peak and trough values for q_β and q_γ charge movements remained similar throughout the spike train, apart from minor differences between the first and subsequent action potentials. The rapid recoveries implied for q_β charge can be explained in terms of its relatively rapid time constants. Similarly, although q_γ has slow on kinetics at small depolarizations, its off kinetics are monotonic and rapid at all voltages (Huang, 1984). Intramembrane processes therefore faithfully follow individual action potentials even with tetanic stimulation frequencies. Hence tetanus has to be attributed to events subsequent to charge transfer.

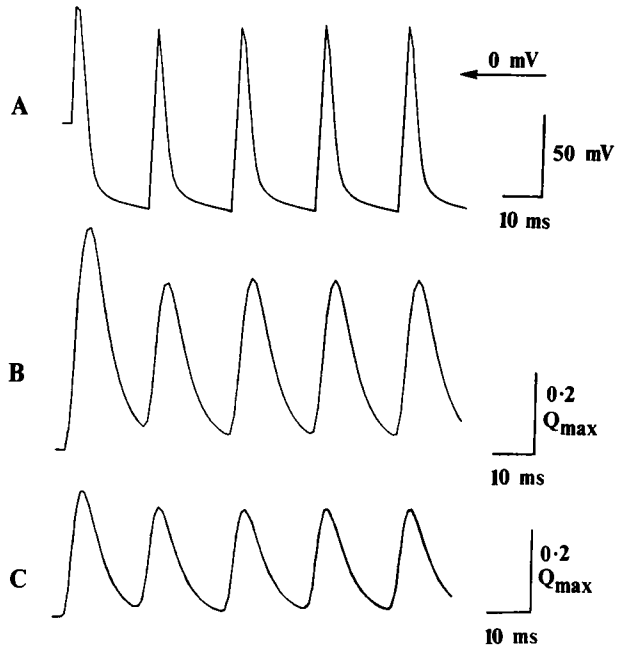

FIGURE 7 Simulation of a train of action potentials (*A*) in response to 1 ms stimuli to −30 mV at a 47.7 Hz frequency ordinarily sufficiently high to cause tetanus. Corresponding traces of charge displaced by q_β (*B*) and q_γ (*C*) summated over all tubular and surface membrane shells are plotted normalized to the maximum available charge.

DISCUSSION

There is accumulating evidence that charge movements in skeletal muscle are causally linked to excitation-contraction coupling in whole or in part. Their kinetic and steady-state properties in response to imposed voltage steps have been characterized in solutions that minimized both the time-dependent ionic conductances and cable attenuations through the transverse tubular system (see, e.g., Adrian and Almers, 1974; Adrian and Peres, 1979; Huang, 1982; Hui, 1983; Horowicz and Schneider, 1981; Melzer et al., 1986; review: Huang, 1988). These experimental conditions were necessary to exclude effects that would arise from cable properties of the tubules, or from ionic conductances in surface or tubular membranes.

However, the actual triggering event for the nonlinear charge in vivo which might thereby activate any subsequent physiological processes, is an action potential initiated in and propagating along the fiber surface and through the transverse tubules. This paper attempts to reconstruct the behavior of the charge under these conditions. It accordingly incorporates intact time and voltage dependent Na and K membrane conductances as well as leak conductances as determined on earlier occasions (Adrian et al., 1970). Adrian and Peachey (1973) described the behavior of a distributed tubular system whose circuit elements were separated from the extracellular fluid by a fixed series resistance. This formulation successfully reproduced the waveform of the surface action potential. Accordingly, a similar approach, simplified to predict regenerative changes following uniform surface stimulation (a "membrane action potential"), was adopted on this occasion.

The original reconstruction of muscle action potentials by Adrian and Peachey (1973) assumed constant specific membrane capacitances. However, charge movements can as much as double membrane capacitance at some voltages (Adrian and Almers, 1976*a*; Duane and

Huang, 1982; Huang, 1982). Accordingly, we first evaluated whether the presence of voltage-dependent capacitance significantly influenced the form of the action potential. We chose values of maximum nonlinear charge that fell in the middle of the range reported in the literature, from studies in which the diameters of the fibers reported were close to that modeled in the present computation (Huang, 1982). In any case, the introduction of nonlinear charge did not greatly affect the magnitude and form of the action potential, certainly not to an extent that would justify modification of either the representation of the tubular system, or the values of series resistances or limiting ionic conductances adopted by Adrian and Peachey (1973). Hence, nor would variations in what are small absolute amounts of maximum nonlinear charge.

We have not modeled the behavior of q_α charge (Adrian and Almers, 1976*a*). However, its broad voltage dependence (e.g., Duane and Huang, 1982) would imply an even smaller influence on the form of the action potential than exerted by q_β or q_γ. Its omission therefore, would not lead to significant error in predicting the voltage changes during regenerative activity, or therefore in deducing the movement of q_β and q_γ.

Tubular cable properties significantly influenced the extent and time course particularly of q_γ charge movement. A greater proportion of either charge species was transferred in tubular membrane near the fiber axis than at the edge. However, in either case, only a fraction (q_γ: 22–34%, q_β, 53–58%) of available charge moved even though the action potential traversed a large fraction of the voltage range through which the charge involved is potential dependent in the steady-state. Comparison of the respective types of model assuming nonlossy and lossy behavior suggested that the larger part of this discrepancy stemmed from dielectric loss properties, particularly for the q_γ component. At all events, such findings would predict differences between either the tension or the $\Delta[Ca^{2+}]$ transient produced by a twitch, and by sustained depolarization, as occurs in a K^+ contracture. Charge movement was also explored for action potential frequencies above 20–40 Hz at 4°C which would normally cause tetanus in frog skeletal muscle. The computed charge movement components faithfully followed individual spikes at least at frequencies up to 47.7 Hz, with no significant charge accumulation.

The q_γ charge movement demonstrated a prominent latency following the onset of the action potential that averaged 2.2 ms over the entire tubular system. Tubular cable properties noticeably influenced the latency at any given site. Thus, latencies were longer in tubular membrane near the fiber axis than at the rim. The predicted latencies were considerably smaller for nonlossy charge. Thus in the case of q_γ, dielectric loss consistently accounted for 1.5 ms of the latency in all regions of the tubular system.

Vergara and Delay (1986) reported that an interval of 3.5–4.5 ms separated the onsets of the action potential and of $\Delta[Ca^{2+}]$ signals at 4°C. Of this latency, Zhu et al. (1986) attributed a minimal interval of 2 ms to tubulocisternal coupling processes taking place beyond the stage of membrane processes and consequently having rates independent of membrane potential. This was based on measurements of Arsenazo III absorbances reflecting changes in myoplasmic $[Ca^{2+}]$ in response to strongly positive voltage steps. Earlier papers have suggested that q_γ is involved in triggering Ca^{2+} release from sarcoplasmic reticulum during excitation-contraction coupling (Huang, 1980, 1981*c*; Vergara and Caputo, 1982; Hui, 1983; Rakowski et al., 1985). If this is so, the latencies exhibited by q_γ charge resulting variously from tubular propagation, membrane charging and loss transients should be compatible with such $\Delta[Ca^{2+}]$ signal latencies. The latency for q_γ charge movement averaged over the entire tubular system following the onset of the surface action potential was 2.2 ms. This offers a significant contribution to the $\Delta[Ca^{2+}]$ signal latency. This is in contrast to q_β charge whose latency even in the center of the tubular system was only 0.3 ms. Taken with the minimal latency of close to 2 ms determined by Zhu et al. (1986: see above), a q_γ charge movement model therefore satisfactorily accommodates the experimentally observed latencies between action potentials, and resulting intramembrane sensing and subsequent coupling events.

Our calculations did not attempt directly to distinguish between chemical (Vergara et al., 1985) or more direct mechanical (Chandler et al., 1976*b*) hypotheses for this coupling. However, they do indicate that the assumption of a physiological role for q_γ charge offers a satisfactory explanation for the empirically observed $\Delta[Ca^{2+}]$ latencies. It additionally yielded preliminary indications for the times required for tubular propagation, membrane depolarization, dielectric loss and tubulecisternal coupling. These could be applied empirically whether the q_γ transition represents an independent event (Adrian and Huang, 1984*b*), or is the end stage in a reaction sequence involving the charge as a whole (Horowicz and Schneider, 1981; Melzer et al., 1986).

We thank Professor R. H. Adrian for helpful discussions and encour-

agement, Mr. W. Smith for artwork and Mrs. Teresa Smith for preparing repeated versions of the manuscript.

Supported by the Royal Society (United Kingdom) and the Muscular Dystrophy Association, Henry M. Watts Neuromuscular Disease Research Center.

Received for publication 2 August 1991 and in final form 2 January 1992.

REFERENCES

Adrian, R. H. 1978. Charge movement in the membrane of striated muscle. *Annu. Rev. Biophys. Bioengin.* 7:85–112.

Adrian, R. H., and W. Almers. 1974. Membrane capacity measurements on frog skeletal muscle in media of low ionic content. *J. Physiol. (Lond.).* 237:573–605.

Adrian, R. H., and W. Almers. 1976*a*. The voltage dependence of membrane capacity. *J. Physiol. (Lond.).* 254:317–338.

Adrian, R. H., and W. Almers. 1976*b*. Charge movement in the membrane of striated muscle. *J. Physiol. (Lond.).* 254:339–360.

Adrian, R. H., W. K. Chandler, and A. L. Hodgkin. 1969*a*. The kinetics of mechanical activation in striated muscle. *J. Physiol.* 204:207–230.

Adrian, R. H., W. K. Chandler, and A. L. Hodgkin. 1970. Voltage clamp experiments in striated muscle fibres. *J. Physiol. (Lond.).* 208:607–644.

Adrian, R. H., L. L. Costantin & L. D. Peachey. 1969*b*. Radial spread of contraction in frog muscle fibres. *J. Physiol.* 204:231–257.

Adrian, R. H., and C. L.-H. Huang, 1984*a*. Charge movements near the mechanical threshold in skeletal muscle of *Rana temporaria*. *J. Physiol. (Lond.).* 349:483–500.

Adrian, R. H., and C. L.-H. Huang. 1984*b*. Experimental analysis of the relationship between charge movement components in skeletal muscle of Rana temporaria. *J. Physiol. (Lond.).* 353:419–434.

Adrian, R. H. and L. D. Peachey. 1973. Reconstruction of the action potential of frog sartorius muscle. *J. Physiol. (Lond.).* 235:103–131.

Adrian, R. H., and A. Peres. 1977. A gating signal for the potassium channel? *Nature (Lond.).* 267:800–804.

Adrian, R. H., and A. Peres. 1979. Charge movement and membrane capacity in frog skeletal muscle. *J. Physiol. (Lond.).* 289:83–97.

Almers, W. 1976. Differential effects of tetracaine on delayed potassium channels and displacement currents in frog skeletal muscle. *J. Physiol. (Lond.).* 262:613–637.

Almers, W. 1978. Gating currents and charge movements in excitable membranes. *Rev. Physiol. Biochem. Pharmacol.* 82:96–190.

Brum, G., and E. Rios. 1987. Intramembrane charge movement in frog skeletal muscle fibres. Properties of charge 2. *J. Physiol. (Lond.).* 387:489–517.

Chandler, W. K., R. F. Rakowski, and M. F. Schneider. 1976*a*. A nonlinear voltage-dependent charge movement in frog skeletal muscle. *J. Physiol. (Lond.).* 254:245–283.

Chandler, W. K., R. F. Rakowski, and M. F. Schneider. 1976*b*. Effect of glycerol treatment and maintained depolarization on charge movement in skeletal muscle. *J. Physiol. (Lond.).* 254:285–316.

Duane, S., and C.L.-H. Huang. 1982. A quantitative description of the voltage-dependent capacitance in frog skeletal muscle in terms of equilibrium statistical mechanics. *Proc. R. Soc. Lond. B Biol. Sci.* 215:75–94.

Eisenberg, R. S. 1983. Impedence measurement of the electrical structure of skeletal muscle. *In* Handbook of Physiology Section 10: Skeletal Muscle. L. D. Peachey, R. H. Adrian, and S. R. Geiger, editors. Am. Physiol. Soc., Bethesda, MD. 301–323.

Gage, P. W., and R. S. Eisenberg. 1969*a*. Capacitance of the surface and transverse tubular membrane of frog sartorius muscle fibers. *J. Gen. Physiol.* 53:265–278.

Gage, P. W., and R. S. Eisenberg. 1969*b*. Action potentials, after-potentials and excitation contraction coupling in frog sartorius fibers without transverse tubules. *J. Gen. Physiol.* 53:298–310.

Horowicz, P., and M. F. Schneider. 1981. Membrane charge movement in contracting and non-contracting skeletal muscle fibres. *J. Physiol. (Lond.).* 314:565–593.

Huang, C. L.-H. 1980. Charge movement components in skeletal muscle. *J. Physiol. (Lond.).* 305:31–32P.

Huang, C. L.-H. 1981*a*. Dielectric components of charge movements in skeletal muscle. *J. Physiol. (Lond.).* 313:187–205.

Huang, C. L.-H. 1981*b*. Membrane capacitance in hyperpolarized muscle fibres. *J. Physiol. (Lond.).* 313:207–222.

Huang, C. L.-H. 1981*c*. Effects of local anesthetics on the relationship between charge movements and contractile thresholds in frog skeletal muscle. *J. Physiol. (Lond.).* 320:381–391.

Huang, C. L.-H. 1982. Pharmacological separation of charge movement components in frog skeletal muscle. *J. Physiol. (Lond.).* 324:375–387.

Huang, C. L.-H. 1983*a*. Experimental analysis of alternative models of charge movement in frog skeletal muscle. *J. Physiol. (Lond.).* 336:527–543.

Huang, C. L.-H. 1983*b*. Time domain spectroscopy of the nonlinear capacitance in frog skeletal muscle. *J. Physiol. (Lond.).* 341:1–24.

Huang, C. L.-H. 1984. Analysis of "off" tails of intramembrane charge movements in skeletal muscle of *Rana temporaria*. *J. Physiol. (Lond.).* 356:375–390.

Huang, C. L.-H. 1986. The differential effects of twitch potentiators on charge movements in frog skeletal muscle. *J. Physiol.* 380:17–33.

Huang C. L.-H. 1987. "Off" tails of intramembrane charge movements in frog skeletal muscle in perchlorate-containing solutions. *J. Physiol.* 384:491–510.

Huang, C. L.-H. 1988. Intramembrane charge movements in skeletal muscle. *Physiol. Rev.* 68:1197–1247.

Huang, C. L.-H., and L. D. Peachey. 1988. The distribution of charge movement components in surface and T-tubule membranes of frog skeletal muscle fibers. *Biophys. J.* 53:604*a*. (Abstr.)

Huang, C. L.-H., and L. D. Peachey. 1989. The anatomical distribution of voltage-dependent membrane capacitance in frog skeletal muscle fibers. *J. Gen. Physiol.* 93:565–584.

Huang, C. L.-H., and L. D. Peachey. 1989. Charge movements during a frog skeletal muscle action potential. *J. Physiol.* 418:121P (Abstr.)

Huang, C. L.-H., and L. D. Peachey. 1990. Reconstruction of charge movement during an action potential. *In* 10th International Biophysics Congress. Proceedings. Vancouver: International Union of Pure and Applied Biophysics. 434.

Hui, C. S. 1983. Pharmacological studies of charge movements in frog skeletal muscle. *J. Physiol.* 337:509–552.

Hui, C. S., and W. K. Chandler. 1991. Q_β and Q_γ components of intramembranous charge movement in frog cut fibers. *J. Gen. Physiol.* 98:429–646.

Melzer, W., M. F. Schneider, B. J. Simon, and G. Szucs. 1986.

Intramembrane charge movement and calcium release in frog skeletal muscle. *J. Physiol. (Lond.).* 373:481–512.

Peachey, L. D. 1965. The sarcoplasmic reticulum and transverse tubules of the frog's sartorius. *J. Cell Biol.* 25:209–231.

Rakowski, R. F., P. M. Best, and M. R. James-Kracke. 1985. Voltage dependence of membrane charge movement and calcium release in frog skeletal muscle. *J. Muscle Res. Cell Motil.* 6:403–433.

Schneider, M. F., and W. K. Chandler. 1973. Voltage-dependent charge in skeletal muscle: a possible step in excitation-contraction coupling. *Nature (Lond.).* 242:244–246.

Vergara, J., and C. Caputo. 1982. Effects of tetracaine on charge movements and calcium signals in frog skeletal muscle fibers. *Proc. Natl. Acad. Sci. USA.* 80:1477–1481.

Vergara, J., and M. Delay. 1986. A transmission delay and the effect of temperature at the triadic junction of skeletal muscle. *Proc. R. Soc. Lond. B Biol. Sci.* 229:97–110.

Vergara, J., R. Y. Tsien, and M. Delay. 1985. Inositol 1,4,5-trisphosphate: a possible chemical link in excitation-contraction coupling in muscle. *Proc. Natl. Acad. Sci. USA.* 82:6352–6356.

Zhu, P. H., I. Parker, and R. Miledi. 1986. Minimal latency of calcium release in frog twitch muscle fibres. *Proc. R. Soc. Lond. B Biol. Sci.* 229:39–46.